DERIVATION OF MAGNETIC ANOMALY MAPS FROM THE MAGSAT MEASUREMENTS

Kýroly I. KIS

Research Group of Geophysics and Environmental Physics
of the Hungarian Academy of Sciences
kisk@ludens.elte.hu

MÁGNESESANOMÁLIA-TÉRKÉPEK LEVEZETÉSE A MAGSAT MÉRÉSEIBŐL

…sszefoglal‡s

A Magsat mesterséges hold méréseiből kerültek levezetésre a vektor és a skalár mágnesesanomália-térképek a 35°– 60° szélességű és -10°– 60° hosszúságú gömbi hálózatban, 400 km magasságban az európai régió területére. Ezeket a vektor és a skalár mágnesesanomália-térképeket a Gauss- és Laplace-féle súlyfüggvények felhasználásával interpoláltuk gömbi hálózatban. A Gauss- és a Laplace-féle súlyfüggvények paraméterei határozzák meg az interpoláció során kezelt legkisebb hullámhosszakat. Az anomáliatérképek levezetése során a legkisebb hullámhosszak 1000 km és 2000 km voltak. A levezetett ΔX, ΔY, ΔZ ąs ΔT térképek jól kifejezik az európai régió regionális mágneses anomáliáit a Magsat magasságában

Summary

Vector and scalar magnetic anomaly maps have been determined from Magsat data on a spherical grid (35°– 60° in latitude and -10°– 30° in longitude) at an altitude of 400 km over the European region. These anomaly maps have been derived using Gaussian and Laplacian weight functions to interpolate the vector and scalar anomaly data. The parameter value of the Gaussian and Laplacian weight functions controls the cut-off wavelength (shortest wavelength) processed by the interpolation procedures. The shortest wavelengths for the derivation of the vector and scalar magnetic anomalies have been set at 1000 km and 2000 km, respectively. The derived ΔX, ΔY, ΔZ, and ΔT maps reflect the regional magnetic anomalies of the European region at the altitude of the Magsat.

Introduction

The U.S. Magsat satellite measured vector and scalar magnetic fields of the Earth following a sun synchronous orbit with inclination 96.76˘ during the period from October 30, 1979 to June 11, 1980 (LANGEL et al., 1982). The results obtained during the last twenty years, the applied data processing, and future perspectives of the satellite magnetic measurements are summarized by LANGEL and HINZE (1998). One of the aims of the Magsat mission was the derivation of magnetic anomaly maps which reflect the magnetic field of crustal origin. Extensive research has been made for the derivation of this kind of magnetic anomaly maps and their interpretation, e.g. FREY (1982), ARKANI-HAMED et al. (1994), RAVAT et al. (1995).

This paper discusses the derivation of vector and scalar magnetic anomaly maps for the European region. It contributes to a series of papers, presenting the scalar and vector anomaly maps of Europe, e.g. ARKANI-HAMED and STRANGWAY (1985) and (1986), TAYLOR and FRAWLEY (1987), RAVAT et al. (1993), TAYLOR and RAVAT et al (1995), KIS and WITTMANN (1998) and (2002), VONIK et al. (2001).

The Magsat data used for the determination of magnetic anomaly maps were filed on Investigator-B magnetic tapes, obtained from the World Data Center A (control number RG 8800). The applied data processing i.e., the corrections and the data selection is the same as published by KIS and WITTMANN (1998) and (2002). The corrected and selected dawn Magsat data set is used for further computations. The spatial distribution of the used data is presented in the mentioned previous papers.

An interpolation procedure forms the basic element for the determination of the scalar and vector anomaly maps. In the next section the applied equations of the interpolation procedure will be introduced. Determination of the parameters of the interpolation procedures is based on the spectral analysis of the satellite anomaly data measured along the individual passes of the satellite. Finally, the implementation of the interpolation procedures and the derived magnetic anomaly maps will be presented.

Interpolation on a spherical grid

Determination of magnetic anomalies from satellite measurements is considered as a problem of interpolation on a spherical grid. The objective of this section is to outline the procedure of the interpolation methods which can be regarded as 3D filtering of the data.

The satellite data measurements ate distributed over three-dimensional spherical shell. The vector ΔX, ΔY, ΔZ, and scalar ΔT anomaly values are obtained by the subtraction of the calculated field values determined from the spherical harmonic model, respectively. This field model (MGS 481#2) was given in the Investigator-B tape for values up to degree and order 14. During this phase of the data processing the magnetic field originating from the Earth's core is removed. In this way the longest wavelength of the anomaly data is also determined, which is approximately 3000 km (BULLARD, 1967).

The interpolation equations are presented for the vector ΔX, ΔY, ΔZ, and scalar ΔT anomaly values in a spherical coordinate system, respectively. The equations are as follows:

$$\Delta X^{interpolated}(r,\theta,\lambda)=\sum_{i=1}^{N} w_i \Delta X^{measured}(r_i,\theta_i,\lambda_i) \quad (1)$$

$$\Delta Y^{interpolated}(r,\theta,\lambda)=\sum_{i=1}^{N} w_i \Delta Y^{measured}(r_i,\theta_i,\lambda_i) \quad (2)$$

$$\Delta Z^{interpolated}(r,\theta,\lambda)=\sum_{i=1}^{N} w_i \Delta Z^{measured}(r_i,\theta_i,\lambda_i) \quad (3)$$

$$\Delta T^{interpolated}(r,\theta,\lambda)=\sum_{i=1}^{N} w_i \Delta T^{measured}(r_i,\theta_i,\lambda_i) \quad (4)$$

where r, θ, λ are the spherical coordinates (radius colatitude, longitude) of the point of interpolation; w_i is the weight of the interpolation for the i-th data; r_i, θ_i, λ_i are the spherical coordinates of the measured point. N is the number of the data used for the interpolation. Data are interpolated for the spherical grid, ranging from 35°–60° in latitude, and -10°–30° in longitude. The increment in latitude and longitude is 0.2˘. The grid is distributed over a sphere with a radius of 6771 km, covering the European region (*Figure 1*). The solution to the interpolation problem includes the determination of the appropriate weight function, and its digitized value, w_i. The interpolation procedure is designed in a three-dimensional spatial frequency domain, and it is implemented in a space domain. The weight function of the interpolation is selected according to the following requirements:

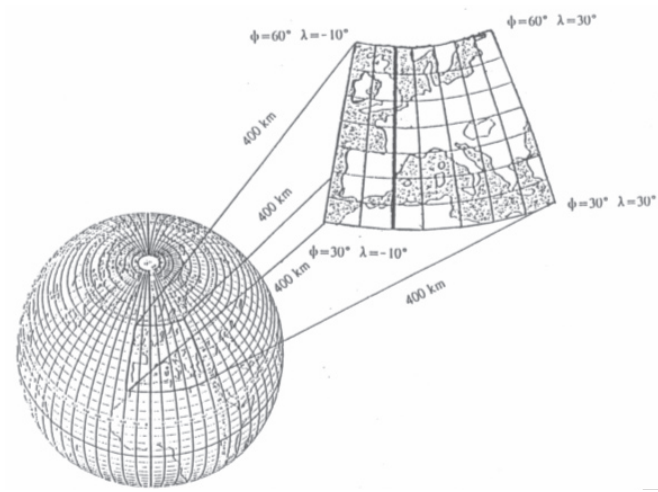

Figure 1. Schematic view of the spherical surface, which is divided into a spherical grid

a) the weight function should be a three-dimensional energy signal, i.e.

$$\int_{-\infty}^{+\infty}\int_{-\infty}^{+\infty}\int_{-\infty}^{+\infty} |w(x,y,z)|^2 \, dxdydz < \infty \qquad (5)$$

and its Fourier transform exists (BRACEWELL, 1978);

b) the weight function should be spherically symmetrical, which is a non-directive transfer property;

c) the low-pass property and its cut-off spatial frequency can be defined.

The Gaussian and Laplacian low-pass filters are subject to the requirements (a), (b), and (c) written above. The Gaussian low-pass filter has the additional advantage that the product of signal-duration and frequency-bandwidth is minimum (BRACEWELL, 1978).

The interpolation is calculated in a three-dimensional Cartesian coordinate system with the x-axis and y-axis oriented North and East, respectively, while the z-axis points vertically downward. The origin of the coordinate system is located at the point at which the value is interpolated. The f_x, f_y, and f_z spatial frequencies are directed in the x-, y-, and z-axis, respectively.

Gaussian and Laplacian low-pass filters

The transfer function of the three-dimensional Gaussian low-pass filter in the spatial frequency domain is

$$S_{Low-pass}^{Gaussian}(f_r, k) = \exp\left(-(kf_r)^2\right), \tag{6}$$

where f_r is the radial spatial frequency, which can be expressed as $f_r^2 = f_x^2 + f_y^2 + f_z^2$. The parameter k controls the cut-off the Gaussian filter.

The cut-off spatial frequency $f_r^{cut-off}$ or the cut-off wavelength $\lambda^{cut-off}$ of the interpolation can be defined by the -3 dB attenuation. The relationship between the cut-off spatial redial frequency or the cut-off wavelength and the parameter k is given by

$$\text{for -3 dB attenuation } \quad f_r^{cut-off} = \frac{0.5887}{k} \quad \text{or} \quad \lambda^{cut-off} = \frac{k}{0.5887}. \tag{7}$$

The weight function of the Gaussian low-pass filter is obtained from the three-dimensional inverse Fourier transform of the transfer function (6):

$$\mathsf{F}^{-1}\{\exp\left(-(kf_r)^2\right)\} = w_{Low-pass}^{Gaussian}(r,k) = \frac{\pi^{3/2}}{k^3}\exp\left(-\left(\frac{\pi r}{k}\right)^2\right), \tag{8}$$

where r is the distance between the point of the spherical grid and the data observed.

The transfer function of the three-dimensional Laplacian low-pass filter in the spatial frequency domain is given by

$$S_{Low-pass}^{Laplacian}(f_r, \mu) = \exp\left(-\mu|f_r|\right), \tag{9}$$

where the parameter μ controls the cut-off spatial frequency. The cut-off spatial frequency of the cut-off wavelength will again defined by the -3 dB attenuation. The relationship between the cut-off spatial frequency or cut-off wavelength and the parameter μ is given by

$$\text{for -3 dB attenuation } \quad f_r^{cut-off} = \frac{0.3466}{k} \quad \text{or} \quad \lambda^{cut-off} = \frac{k}{0.3466}. \tag{10}$$

The weight function of the Laplacian low-pass filter can obtained now from the three-dimensional Fourier transform of the transfer function (9):

$$\mathsf{F}^{-1}\{\exp\left(-\mu|f_r|\right)\} = w_{Low-pass}^{Laplacian}(r,\mu) = \frac{8\pi\mu}{\left(\mu^2 + 4\pi^2 r^2\right)^2}. \tag{11}$$

For numerical calculations, the dimensionless spatial frequency f_r' and the dimensionless parameters k' and μ'; and the dimensionless variable r' are introduced as

$$f_r' = f_r\xi,\ k' = k/\xi,\ \mu' = \mu/\xi, \text{ and } r' = r/\xi$$

where ξ is the sampling interval. The average distance of the measurements over the spherical shell for the dawn data is approximately 40 km.

The transfer function of the Gaussian low-pass filter is displayed on a surface plot versus the dimensionless spatial frequencies f_x' and f_y' for $f_z' = 0$ and $f_z' = 0.02$, respectively (*Figure 2*). For a cut-off wavelength of 1000 km, the value of the parameter k' is 14.71 (*Equation (7)*). The solid horizontal contour in *Figure 2* indicates the value of the -3 dB attenuation of the transfer.

The transfer function of the Laplacian low-pass filter is displayed on a surface plot versus the dimensionless spatial frequencies f_x' and f_y' for $f_z' = 0$ and $f_z' = 0.02$, respectively (*Figure 3*). For a cut-off wavelength of 1000 km, the value of the parameter μ' is 8.66 (*Equation (10)*). The solid horizontal contour in *Figure 3* indicates the value of the -3 dB attenuation of the transfer.

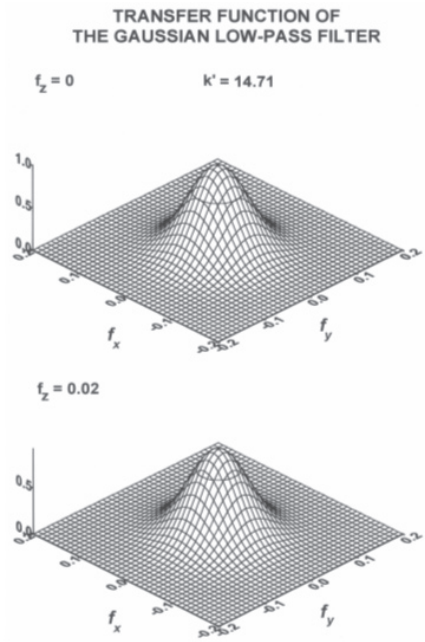

Figure 2. Surface plot of the transfer function of the Gaussian low-pass filter (the value of the parameter k′ is 14.71) versus the dimensionless spatial frequencies f_x' and f_y', and the spatial frequency f_z' is set to 0 and 0.02, respectively. Horizontal contour shows the -3 dB attenuation

Magnetic anomaly maps

The vector and scalar magnetic anomaly maps as derived from our interpolation procedure for a spherical grid are presented in this section. The altitude of the spherical grid is 400 km which corresponds to the average altitude of the Magsat satellite. The radius of the three-dimensional sphere (which surrounds a grid point) is determined by the decrease of the weight function for its 0.01 fraction. This requirement determines the number of the data points used for interpolation.

The corresponding values of the parameters k' and μ' were obtained from the power spectrum of the analyzed pass sections. A value of 1000 km is considered an appropriate shortest wavelength based on the spectrum analysis of the passes. The Gaussian low-pass filter was applied as the weight function of the interpolation procedure to derive the ΔX, ΔY, ΔZ, and ΔT magnetic anomaly maps shown in *Figure 4*. These maps represent the regional character (for the wavelength range between 3000 km and 1000 km) of magnetic anomalies over the European region at satellite altitude.

The total magnetic anomaly for the European region, shown in *Figure 4* is derived using the Laplacian weight function interpolation procedure with a cut-off wavelength set at 2000 km, The parameter value μ' is 17.33 accordingly set to. The regional character (for the wavelength range between 2000 km and 3000 km) of the total magnetic anomalies present in the European region can be clearly seen.

The interpolation of the ΔZ anomalies determined by the suggested method was discussed by KIS and WITTMANN (1998), (2002). The following characteristic regional magnetic anomalies can be recognized in *Figure 4* and *Figure 5*. The Tornquist–Teisseyre tectonic line is indicated by a high gradient zone in the northeast part of the ΔZ and ΔT maps. A large magnetic low can be seen in the middle part of the European continent. It correlates with the north Germano–Polish depression which is called the Central European Magsat low by RAVAT et al. (1993). The magnetic high zone (in the central part of the vertical magnetic anomaly map and a relative high zone (in the central part of the vertical

magnetic anomaly map and a relative high zone in the central part of the total magnetic anomaly maps) is located in the south of Italy. They correspond to the area of low heat flow a thicker lithosphere.

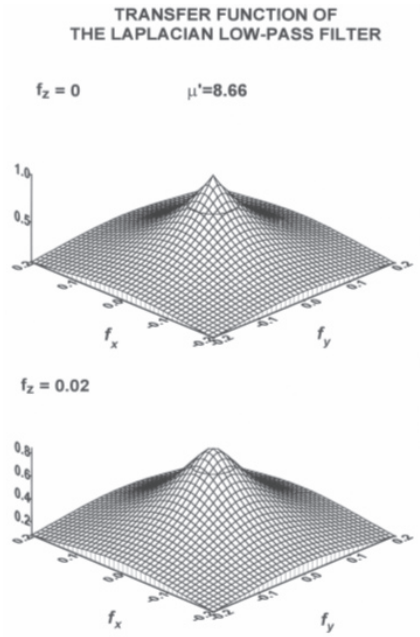

Figure 3. Surface plot of the transfer function of the Laplacian low-pass filter (the value of the parameter μ′ is 8.66) versus the dimensionless spatial frequencies f_x' and f_y', and the spatial frequency f_z' is set to 0 and 0.02, respectively. Horizontal contour shows the -3 dB attenuation

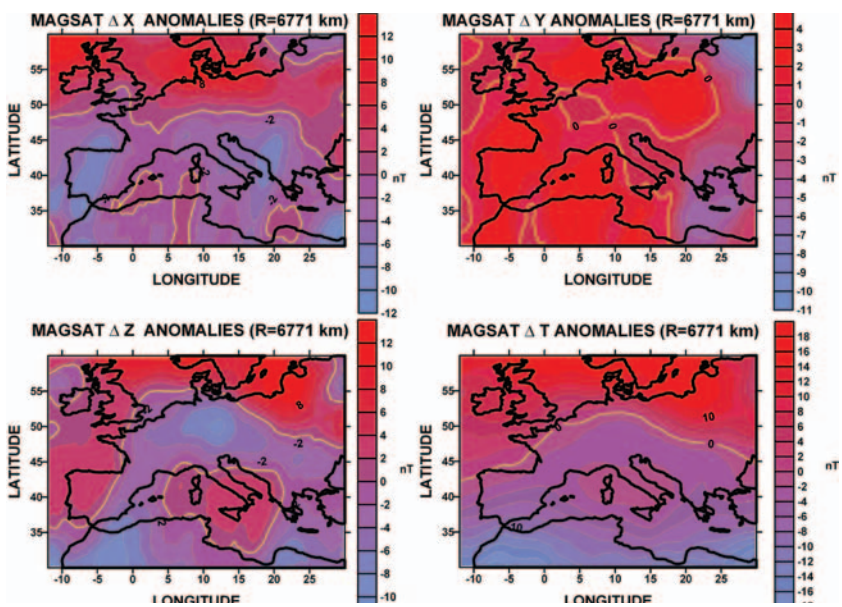

Figure 4. Contour plots of interpolated vector and scalar anomalies (the Gaussian weight function is applied for the interpolation) for the European region on a sphere with radius of 6771 km. The contour interval is 2 nT, while negative values are indicated by downhill hachures, plotted on an equidistant cylindrical projection

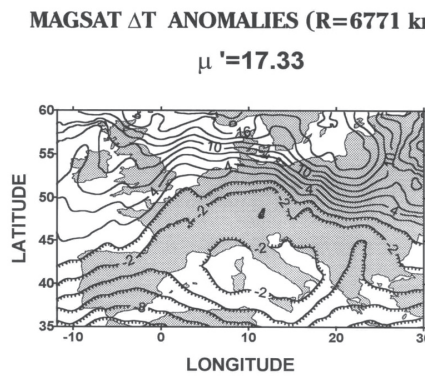

Figure 5. A contour plot of interpolated scalar anomalies (the Laplacian weight function is applied for the interpolation) for the European region on the surface of a sphere of radius 6771 km. The contour interval is 2 nT, while negative values are indicated by downhill hachures, using an equidistant cylindrical projection

References

ARKANI-HAMED, J. – STRANGWAY, D. W.: *Intermediate-scale magnetic anomalies of the Earth.* Geophysics, 50, 1985. 2817–2830. p.

ARKANI-HAMED, J. – STRANGWAY, D.W.: *Magnetic susceptibility anomalies of lithosphere beneath eastern Europe and the Middle East*. Geophysics, 51, 1986. 1711–1724. p.

ARKANI-HAMED, J. – LANGEL, R.A. – PURUCKER, M.: *Scalar magnetic anomaly maps of the Earth derived from POGO and Magsat data.* Journal of Geophysical Research. 99 (B12), 1994. 24075–24090. p.

BRACEWELL, R.N.: *The Fourier Transform and its Applications.* 1978. McGraw–Hill Book Co.

BULLARD, E. C.: *The removal of trend from magnetic surveys.* Earth and Planetary Science Letters, 2, 1967. 293–300. p.

FREY, H.: *Magsat scalar anomaly distribution*. Geophysical Research Letters, 9, 1982. 277 - 280 p.

KIS, K.I. – WITTMANN, G.: *Determination of vertical magnetic anomalies and equivalent layer for the European region from the Magsat measurements.* Journal of Applied Geophysics, 39, 1998. 11–24 p.

KIS, K.I. – WITTMANN, G.: *3D reduction of satellite magnetic measurements to obtain magnetic anomaly coverage over Europe*. Journal of Geodynamics, 33, 2002., 117-129. p.

LANGEL, R.A. – OUSLEY, G. – BERBERT, J. – MURPHY, J. – SETTLE, M.: *The Magsat mission.* Geophysical Research Letters, 9, 1982. 243–245. p.

LANGEL, R. A. – HINZE, W. J.: *The Magnetic Field of the Earth's Lithosphere, the Satellite Perspective.* 1998. Cambridge University Press.

RAVAT D. N. – HINZE, W.J. – TAYLOR, P.T.: *European tectonic features observed by Magsat.* Tectonophysics, 220, 1993. 157–173. p.

RAVAT, D.N. – LANGEL, R.A. – PURUCKER, M. – ARKANI-HAMED, J. – ALSDORF, D.E.: *Global vector and scalar Magsat magnetic anomaly maps*. Journal of Geophysical Research, 100 (B10), 1995. 20111–20136. p.

TAYLOR, P.T. – FRAWLEY, J.J.: *Magsat anomaly data over the Kursk region, U.S.S.R.* Physics of the Earth and Planetary Interiors, 45, 1987. 255–265 p.

TAYLOR, P.T. – RAVAT D. N.: A*n interpretation of the Magsat anomalies of central Europe*. Journal of Applied Geophysics, 34, 1995. 83–91. p.

VONIK, T. – TRIPPLER, K. – GEIPEL, H. – GREINWALD, S. – PASHKEVITS, I.: *Magnetic anomaly map for Northern, Western, and Eastern Europe.* Terra Nova, 13, 2001. 203–213 p.